

Available online at website: https://journal.bcrec.id/index.php/bcrec

Bulletin of Chemical Reaction Engineering & Catalysis, 20 (3) 2025, 483-492



Original Research Article

Nanostructured Ni-B Seed Layer Electrocatalysts for Oxygen Evolution Reaction

Taghi Morshedlo, Seyed Alireza Hosseini*, Mohammad Hossein Shahini, Soghra Ghorbanzadeh, Mostafa Alishahi

Department of Materials and Polymer Engineering, Faculty of Engineering, Hakim Sabzevari University, Iran.

Received: 14th May 2025; Revised: 3rd July 2025; Accepted: 7th July 2025 Available online: 30th July 2025; Published regularly: October 2025



Abstract

The current study investigates the electrocatalytic activity of the nanostructured Ni-B seed layer deposited on carbon paper for the oxygen evolution reaction. Accordingly, the influence of several fabrication parameters and post-heat treatment on the electrocatalytic behavior of the samples is studied. Nanostructure seed Ni-B/CP electrodes were synthesized by an electroless deposition method, and a uniform layer of nanostructure seeds was obtained after 120 s of deposition time. Results have shown by the rising B content the catalytic properties of the Ni-B/CP electrodes are enhanced. The catalytic activity for OER diminished after heat treatment at 400 °C for 1 h.

Copyright © 2025 by Authors, Published by BCREC Publishing Group. This is an open access article under the CC BY-SA License (https://creativecommons.org/licenses/by-sa/4.0).

Keywords: Nanostructured Ni-B layer; electroless; electrocatalysts; oxygen evolution reaction (OER)

How to Cite: Morshedlo, T., Hosseini, S. A., Shahini, M. H., Ghorbanzadeh, S., Alishahi, M. (2025). Nanostructured Ni-B Seed Layer Electrocatalysts for Oxygen Evolution Reaction. Bulletin of Chemical Reaction Engineering & Catalysis, 20 (3), 483-492. (doi: 10.9767/bcrec.20392)

Permalink/DOI: https://doi.org/10.9767/bcrec.20392

1. Introduction

A primary concern of recent decades is the environmental damage caused by the huge consumption of fossil fuels. Harnessing the capacity of hydrogen as a green alternative to conventional fuels has been the center of many studies in recent years. Hydrogen fuel possesses high energy potential, high storage capability, and environmental friendliness. As a green path for hydrogen production, water-splitting reaction has captured the attention of scientists in recent years. Like the other electrochemical reactions, the water splitting is divided into two halfreactions: oxygen evolution reaction (OER) at the anode and hydrogen evolution reaction (HER) at the cathode [1]. Since water splitting requires high activation energy to occur, the employment of electrocatalysts is inevitable. This is more highlighted in the anodic half-reaction or OER, where the formation of each oxygen gas molecule is dependent on the transfer of four electrons. The electrocatalysts can impact the reaction kinetics, boost the reaction rate, and reduce the production cost. Hence, developing new catalysts capable of speeding up the water-splitting process is of key importance. RuO2, IrO2, and Pt are known as effective electrocatalysts for water splitting; nevertheless, due to their rare existence and cost issues, considerable efforts have been made to discover alternatives [2]. Such a target can be achieved by employing transition metals like Ni, Fe, and Co and, in particular, their hydroxide and oxide compounds [3,4], or their compounds with nonmetallic components such as P. N. Se, S, and B. Among all the potential candidates, Ni-based compounds have attracted attention due to their high catalytic activity, high stability in different

* Corresponding Author. Email: sar.hosseini@hsu.ac.ir (S. A. Hosseini)

media, and cost-effectiveness. For an excellent instance, the electrocatalytic activity of the Ni₂P, Ni₅P₄, NiSe, NiFe, and Ni₃N has been reported to be good compared to RuO₂, IrO₂, and Pt [5,6].

Different methods could be applied to obtain an electrocatalytic layer on the electrode for water-splitting systems. Electroless deposition is a facile and low-cost method for forming metallic like Ni-based films. electrodeposition, it requires no electricity, and a reducing agent added to the metallic salt reduces the metallic ions and forms the coating layer on the substrate. An important advantage of the electroless technique is the uniform covering of the pores and edges of the substrate. Depending on the composition of reducing agents (e.g., NaH₂PO₂ or NaBaH₄), phosphorus and boron could be incorporated into the metallic layer [7,8]. Ni-B coatings are famous for their high mechanical properties, corrosion resistance, and low electrical resistance; however, recent research has proven their extraordinary catalytic activity to produce hydrogen, which could be comparable with Pt performance [9-12]. Zeng et al. [9] researched the Ni-B electrocatalytic properties, and their results were suggestive of its great efficiency and stability for HER in a wide range of pH. Edison et al. [13] used the ultrasonic method to synthesize Ni-B nanorods. The outcome revealed the sophisticated catalytic functionality of the nanorods for OER in the KOH environment. In another investigation, Liang and coworkers [14] researched the application of Ni-B on the Ni foam through an electroless technique to probe into its potential catalytic activity. The results demonstrated that the provided 3D catalyst electrode exhibited great stability and activity for HER and OER.

As a rule of thumb, among all the Ni-based compounds consisting of metalloids (e.g., B, Si, As, Te) as well as P, the best catalytic properties for the OER reaction are conferred on B [15]. A few researchers focused on Ni-based compounds with B, there have been limited studies concerned on method. Therefore, this research intends to investigate and maximize the OER

electrocatalytic activity of the Ni-B layer fabricated via electroless technique, by using porous carbon paper (CP) substrate and controlling deposited seed layer morphology at the nanoscale. In the current study, the influence of various factors such as electroless plating time, B concentration, and post-heat treatment on the electrocatalytic properties of the prepared Ni-B/CP electrodes was investigated.

2. Materials and Method

2.1 Fabrication of Ni-B/CP Electrocatalysts

Carbon papers (CPs) were cut into a size of 1×1 cm2 and then ultrasonicated in acetone and ethanol for 10 min. The Ni-B electroless layers were deposited on CP for several deposition times (30, 120, and 240 s), where the NaBH₄ concentration was 500 and 1000 mg/L. Also, a polished copper (PC) sample was coated with Ni-B for the sake of comparison. One selected sample was heat-treated at 400 °C for 1 h. The sample designation is listed in Table 1. The deposition times (30, 60, 120, 240 s) and NaBH₄ concentrations (500-1000 mg/L) was based on a combination of literature precedent preliminary bath optimization, our preliminary experiments confirmed that within this window, coatings exhibited measurable differences in thickness, morphology, and OER activityvalidating the utility of these conditions for systematic investigation [16,17].

2.2. Characterization of the Electrodes

The morphology and chemical composition of the deposited layer were examined by scanning electron microscopy (SEM) and energy dispersive spectroscopy (EDS), respectively. The phase structure of the selected Ni-B layer before and after heat treatment was investigated by X-ray diffraction (XRD) using a diffractometer (Philips Expert, Germany) with a Cu-Kα radiation (wavelength of 0.154 nm by using a 1D detector with a rate of 1 s/step.

Table 1. Samples designation and their deposition parameters.

Designation	Substrate	Deposition time (s)	NaBH ₄ concentration (mg/L)	Heat treatment	Constant parameters
NBB	PC	120	500	-	NiCl ₂ (Nickel(II) chloride hexahydrate, purists.
NB30	CP	30	500	-	p.a., ≥98%): 25 g/L
NB60	CP	60	500	-	NaOH (BioXtra, \geq 98% (acidimetric)); 40 g/L
NB120	CP	120	500	-	Etylendiamine (EDA>99%): 60 mg/L
NB240	CP	240	500	-	Pb (NO ₃) ₂ (Lead(II) nitrate, ACS reagent, ≥99.0%): 20 mg/L
NB120H	CP	120	500	400 °C 1 h	T= 90-95 °C
NHB120	CP	120	1000	-	pH = 13.5

2.3. Electrochemical Measurements

Electrochemical experiments were performed IVIUM Compactstat potentiostat instrument in 1 M KOH solution. A threeelectrode system consisting of the fabricated electrodes, a saturated calomel electrode (SCE), and a platinum sheet as working, counter, and reference electrodes was employed (Figure 1). Linear sweep voltammetry (LSV) tests were conducted within the potential range of 100-1000 mV to SCE at a scan rate of 10 mV/s. A cyclic voltammetry (CV) test in the 900-1000 mV (vs. RHE) range was employed to obtain the electrochemically active surface area (ECSA) value, which determines the real active surface of the electrocatalysts. Moreover, the ECSA = Cdl/Cs equation is applied to achieve the ECSA value, where the Cdl double-layer capacitance of the electrodes and Cs serves as the double-layer capacitance for a completely flat electrode with 1 cm² area (which is usually considered 0.040 mF.cm⁻²) [17]. To calculate the Cdl, the difference between the anodic and cathodic current ($\Delta j = ja - jc$) at the potential of 1 V (vs. RHE) was calculated at different scan rates; then the Cdl value was obtained by utilizing the Cdl = $d\Delta j/2dV$ equation. electrochemical the impedance spectroscopy (EIS) was performed at 600 mV (vs. SCE), and the frequency range was from 0.01 to 100000 Hz with the perturbation of 10 mV.

3. Results and Discussion

3.1. Surface Morphology and Composition of Electrodes

Surface morfphology and EDS map analysis results of the Ni-B layer after 120 s of the electroless process are depicted in Figures 2 and 3. The results indicate the existence of Ni, B, O, and Pb elements. The chemical composition of the layer is composed of around 64.7 at.% of Ni, 21.4

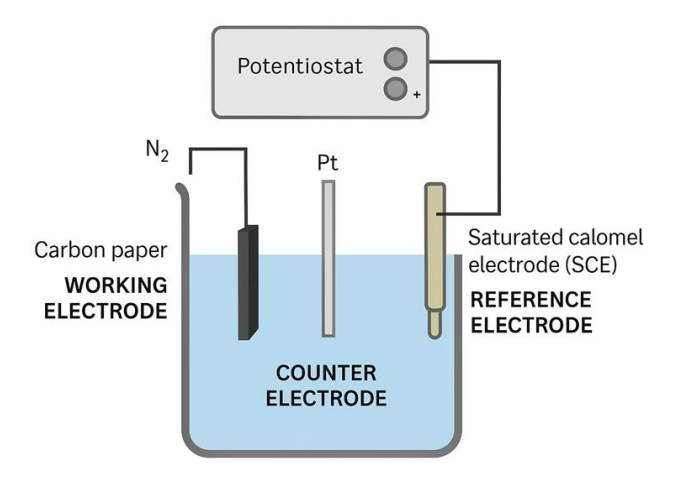


Figure 1. Schematic diagram of electrochemical measurement testing.

at.% of B, and a small amount of C, Pb, and O. The carbon can originate from the CP substrate and surface contaminations. The presence of Pb is associated with the lead nitrate in the solution used as a stabilizer [18]. Also, oxygen presence can be relevant to the innate surface oxidation of the Ni-B layer. The B: Ni atomic ratio regarding the sample fabricated in a solution containing 500 mg/L NaBH₄, was 0.33, denoting the significant contribution of B in the layer. The uniform distribution of Ni and B elements is shown in the EDS map. Also, EDS results reveal that doubling the NaBH₄ amount in the solution to 1000 mg.L-1 causes the increment of B content in the deposited

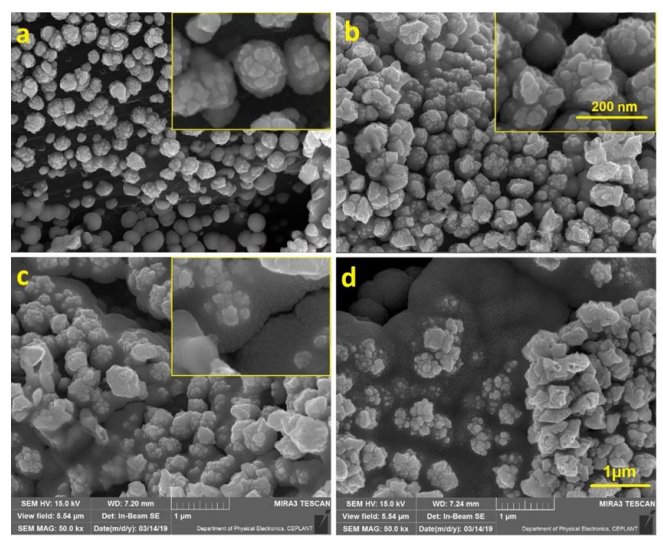


Figure 2. SEM micrographs of the surface of the electrode after different plating times: a) NB30, b) NB60, c) NB120, and d) NB240.

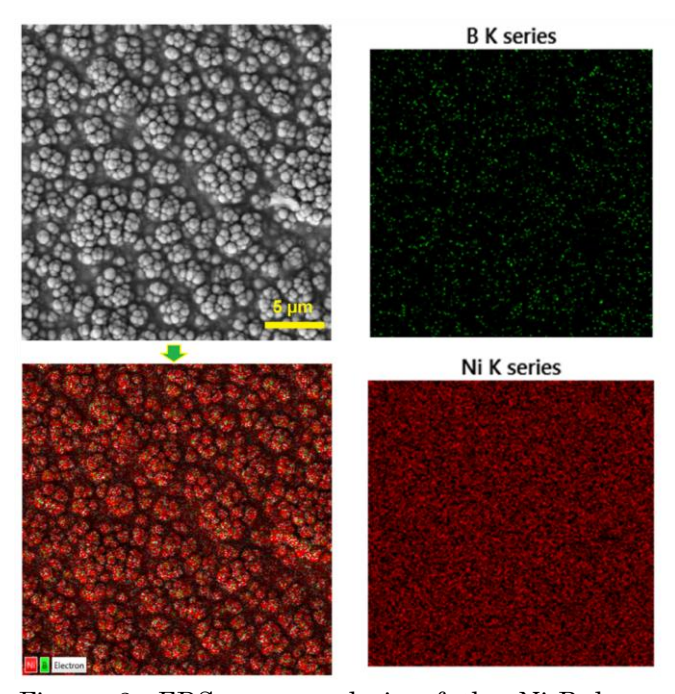


Figure 3. EDS map analysis of the Ni-B layer deposited on CP by the electroless process.

layer from 21.4 to 43.3 3 at.%, and the B: Ni atomic ratio was augmented to 1.17. Pb contamination can severely impact both the catalytic properties and stability of catalysts in the oxygen evolution reaction (OER). Pb²⁺ can adsorb onto the catalyst surface, blocking active sites and lowering OER activity and can alter the electronic structure of surface atoms (e.g., Ni, Co, Fe). The amount of the impurity is a key factor in this regard, and having a higher amount of Pb than >0.01 wt% (100 ppm) is likely to inhibit OER activity and degrade performance measurably. The amount of the impurity here is less than 100 ppm, so we do not see any reduction in OER activity.

Figure 4 represents the XRD patterns of the NB120 sample before and after the heat treatment for 1 h at 400 °C. The presence of a broad single peak around $2\theta = 45^{\circ}$ in the XRD pattern of untreated NB120 is due to an amorphous and nanostructured structure [19]. According to the Ni-B phase diagram, B is insoluble in the Ni structure in an equilibrium state [20]. Hence, a high B content in the nickel matrix leads to the formation of a supersaturated solid solution and gives rise to the amorphous Also, the shift of the corresponding to the Ni (111) plane to higher diffraction angles demonstrates the formation of the Ni-B solid solution. The presence of B in the Ni matrix as a substantial element results in a decrease in lattice parameters and shifts the Ni peak to higher diffraction angles. After heat treatment at 400 °C for 1 h, the structure becomes crystalline, and sharp peaks of different crystallographic planes have appeared. Also, supersaturated B could be released from the Ni matrix through diffusion and precipitate in the form of the Ni₃B phase [21]. The precipitation of the Ni₃B phase causes a decrease of dissolved B in the layer, an increase in lattice parameters, and a shift of the XRD peak to the lower angles (The magnified graph).

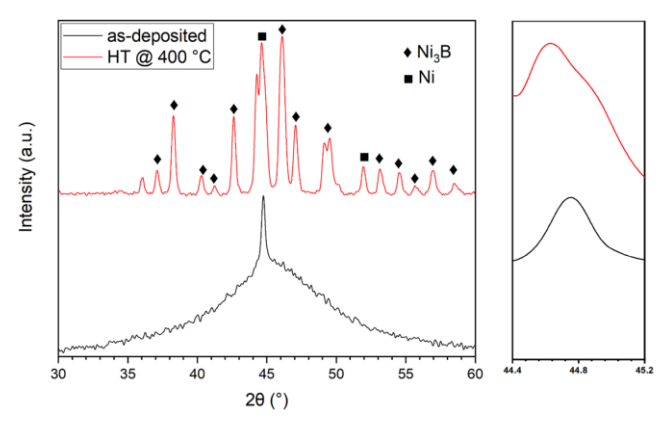


Figure 4. XRD patterns of the Ni-B deposited layer (NB120) before and after heat treatment at 400 °C for 1 h.

3.2. Electrocatalytic Behavior of the Samples

3.2.1 The effect of deposition time

The electrocatalytic activity of the Ni-B/CP electrodes fabricated by different deposition times was investigated using polarization tests in the KOH (1 M) solution. Figure 5A-B represents the LSV curves and corresponding Tafel plot results. In the water-splitting process, the equilibrium potential of the OER was 1.23 V (vs. RHE); however, the reaction is unable to initiate at this potential due to the energy barrier, and it necessitates the activation energy. This energy can be supplied through overpotential (η) . A good electrocatalyst for the water-splitting process could significantly reduce the OER and/or HER overpotential. According to LSV results, the deposition of the Ni-B layer on the CP shifted the graphs to the left- versus the unloaded-CP. Also, the comparison of the graphs revealed that the Ni-B layer applied on the CPs yielded a superior catalytic performance compared to the sample with a Cu substrate. This correlates to the higher specific surface area of the CPs. Moreover, the initial peak (1.4 V) for the oxidation of Ni²⁺ to Ni³⁺conversion of Ni(OH)₂ to NiOOH- is significantly more intense for the Ni-B layer on CPs. The intensity of the peak was also increased with deposition time to 120 s, and further increasing to 240 s, the intensity was reduced. It seems that the development of the Ni-B layers to 120 s promotes the pre-oxidation reaction.

Also, the LSV graphs shift to the lower potentials with increasing deposition time up to 120 s, which reflects the improvement of the electrocatalytic activity for the OER. For a more detailed comparison, some parameters consisting of the overpotential at current densities of 10 and

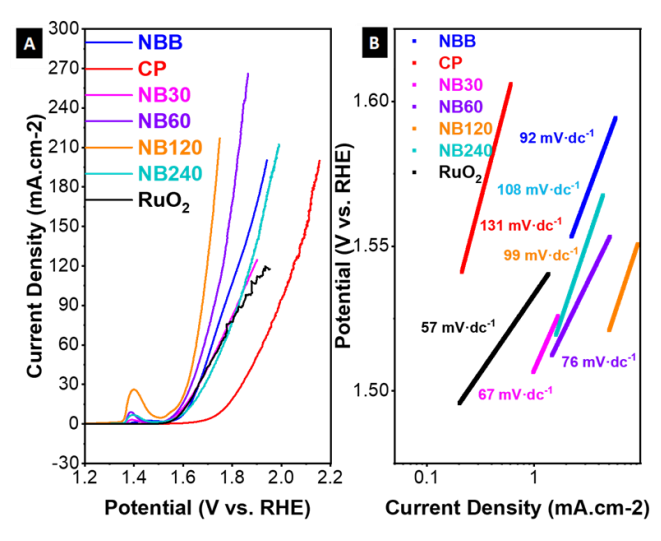


Figure 5. A) The LSV plots of the Ni-B/CP electrodes with different deposition times in 1 M KOH solution with a pH of 14 and B) corresponding Tafel plots of studied electrodes.

100 mA/cm² ($\eta_{i=10}$ and $\eta_{i=100}$, respectively) are extracted from the LSV curves and tabulated in Table 2. The drastic drop in the overpotentials after 30 s deposition time is correlated with the formation of Ni-B seeds on the carbon paper and the change of surface characteristics. increment of deposition time to 120 s resulted in a decrement in the η_{10} and η_{100} values, leading to the enhancement of the electrocatalytic performance. During this period, the seeds grow, join together, and subsequently cover the whole of the CP surface. The best results were obtained for the NB120 sample, in which $\eta_{i=100}$ and $\eta_{i=100}$ are 320 and 450 mV, respectively. The overpotential values increased with the prolonging of deposition time from 120 to 240 s, indicating a decrease in electrocatalytic activity. Further rise of deposition time encouraged the deposition of the nickel atoms on initial seeds and reduced the specific surface area. As mentioned before, Ni-B layer formation follows an initial lateral growth and layer-by-layer process in which the increase of deposition time prompts the formation of new seeds above the previously grown ones, resulting in the active surface decrement. As the electrochemical reactions occur on the surface of electrodes; hence, decreasing the surface area can decrease the reaction rate and thus the catalyst efficiency [22].

In addition, the Tafel slope provides beneficial information about the rate-limiting step of the OER process. Generally, in alkaline solutions, the reaction proceeds through a multi-step process to convert OH to O₂ [23]. The reaction is given by:

$$0H^- \rightarrow 0_2 + 2H_20 + 4e^-$$
 (1)

$$* + OH^{-} \rightarrow *OH^{-} + e^{-}$$
 (2)

$$* OH^- + OH^- \rightarrow * O + H_2O + e^-$$
 (3)

$$* 0 + 0H^{-} \rightarrow * 00H + e^{-}$$
 (4)

$$* 00H + 0H^{-} \rightarrow * +0_{2} + H_{2}O + e^{-}$$
 (5)

The first step is an electron transfer process, if it is a rate-determining step, the Tafel slope is about 120 mV.dec⁻¹. The second stage is slightly

Table 2. Electrocatalytic parameters obtained from electrochemical experiments for different electrodes.

Designat ion	η ₁₀ (mV)	η ₁₀₀ (mV)	Tafel slope (mV.dec ⁻¹)	$C_{ m dl} \ ({ m mF } { m c} \ { m m}^{-2})$	ECSA
CP	528	782	131	0.11	4.4
NBB	383	558	92	0.17	2.8
NB30	347	527	67	0.15	3.8
NB60	347	508	76	0.36	9.4
NB120	320	450	99	0.90	22.5
NB240	383	613	108	0.25	6.3
NB120H	330	470	133	1.94	48.5
NHB120	-	430	89	1.13	28.3
RuO_2	360	640	57	-	-

more complicated, and if this stage is the ratedetermining step, the corresponding Tafel slope is reduced to 60 mV, while if an electron-proton reaction is rate-determining, the Tafel slope is reduced to 40 mV. As shown in the figure, by coating Ni-B on CP, different Tafel slopes are observed, all of which are less than 120, which indicates that the second step reaction determines the rate [24,25].

Electrochemical active surface area (ECSA) is a term used to define the surface area involved in such electrochemical reactions. A technique used for defining the ECSA is the CV in different scan rates at the non-faradic potential region in which the faradic current is negligible [26-28]. The Cdl and ECSA values for different samples obtained from the CV test were collected in Table 2. Results revealed that the maximum ECSA value of 22.5 was obtained for the NB120 sample, which is more than 8 times that of the flat Ni-B layer deposited on the polished copper disk. Also, the value for the samples with 30, 60, and 240 s of deposition times is lower (3.8, 9.4, and 6.3, respectively), which is consistent with microstructural observations and the catalytic activity of the electrodes. Variations in ECSA directly influence catalytic performance because ECSA reflects the active sites available for reaction. A higher ECSA generally means more catalytic sites, leading to increased activity, better reaction rates, and improved efficiency. Conversely, a lower ECSA reduces the number of accessible active sites, limiting performance. However, it's crucial to consider that not only the quantity but also the quality and accessibility of these active sites affect catalysis. Thus, while ECSA is a strong indicator, catalytic performance also depends on catalyst structure, morphology, and stability. In this regard, as shown in Table 2, the catalyst structure and morphology by increasing the time to 120 s, which can increase the active size and improve the quality and accessibility of these active sites. However, by increasing the deposition time to 240 s, on the one hand, the quantity was increased; on the other hand, the catalytic activity was decreased, which can be attributed to the reduction in the quality and accessibility of these active sites.

Nyquist plots obtained from EIS measurements, which are shown in Figure 6, confirmed the LSV results. The fitting parameters obtained based on the equivalent circuit model are collected in Table 3. The R3 represents the charge transfer resistance (Rct) and is related to the electron transfer kinetics at the surface of the electrode. The Rct values obtained for the NBB, CP, NB120, and NB240 are 2.84, 40.81, 1.81, and 6.99 ohms/cm², respectively. The inductive loop is shown in the Nyquist plots at intermediate frequencies, and it can be attributed to the adsorption of abundant amounts hydrogen

amount of hydrogen. For fitting by Zview software, an adsorbent inductance and an adsorbent resistance are added to the equivalent circuit [29,30]. The results indicate that the NB120 sample shows the lowest resistance against the electron transfer and the maximum charge transfer rate, implying the best electrocatalytic performance.

3.2.2 The effect of NaBH₄ concentration

The LSV curves and corresponding Tafel plot of the deposited Ni-B layer fabricated in the electroless solutions containing 500 and 1000 mg of NaBH₄ reducing agent are shown in Figure 7a. It can be seen that increasing NaBH₄ in the bath (NHB120 sample) improves the OER catalytic activity, in which $\eta_{i=100}$ of the electrodes were dropped from 450 to 430 mV. As mentioned before,

an increase in the NaBH₄ concentration leads to an increase in the B: Ni atomic ratio in the deposited layer from 0.33 to 1.17. It seems that the increase in the B concentration in the structure improves the catalytic activity. Similar results were reported about the catalytic activity of Ni-B electroless films for HER [10]. Moreover, the intensity of the pre-oxidation peak significantly increases with B concentration, implying enhancement of the Ni²⁺ to Ni³⁺ reaction.

3.2.3 The effect of post-heat treatment

The effect of post-heat treatment on the catalytic activity of the Ni-B layer is depicted in the LSV curves of Figure 7b. It is obvious that heat treatment decreased the electrocatalytic properties and increased the η_i =100 from 450 to 490 mV. During heat treatment, the amorphous

Table 3. The fitting parameters for different electrodes were obtained based on equivalent circuit models using ZView software.

Sample	Equivalent circuit	R1 (Ω.cm²)	C1	L1	R2 $(\Omega.cm^2)$	CPE1-T (F) (mF.cm ⁻²)	CPE1- P	R3 (Ω .cm ²)
CP	R1 C1 CPE1	1.60	0.00007	-	0.7	0.00252	0.93	40.81
NBB	R2 R3	0.65	0.00054	-	0.09	0.00796	0.84	2.84
NB120	R1 C1	1.72	0.00012	0.00030	1.0	0.08152	0.90	1.81
NB240	L1 CPE1	1.87	0.00008	0.00056	1.26	0.03544	0.59	6.99

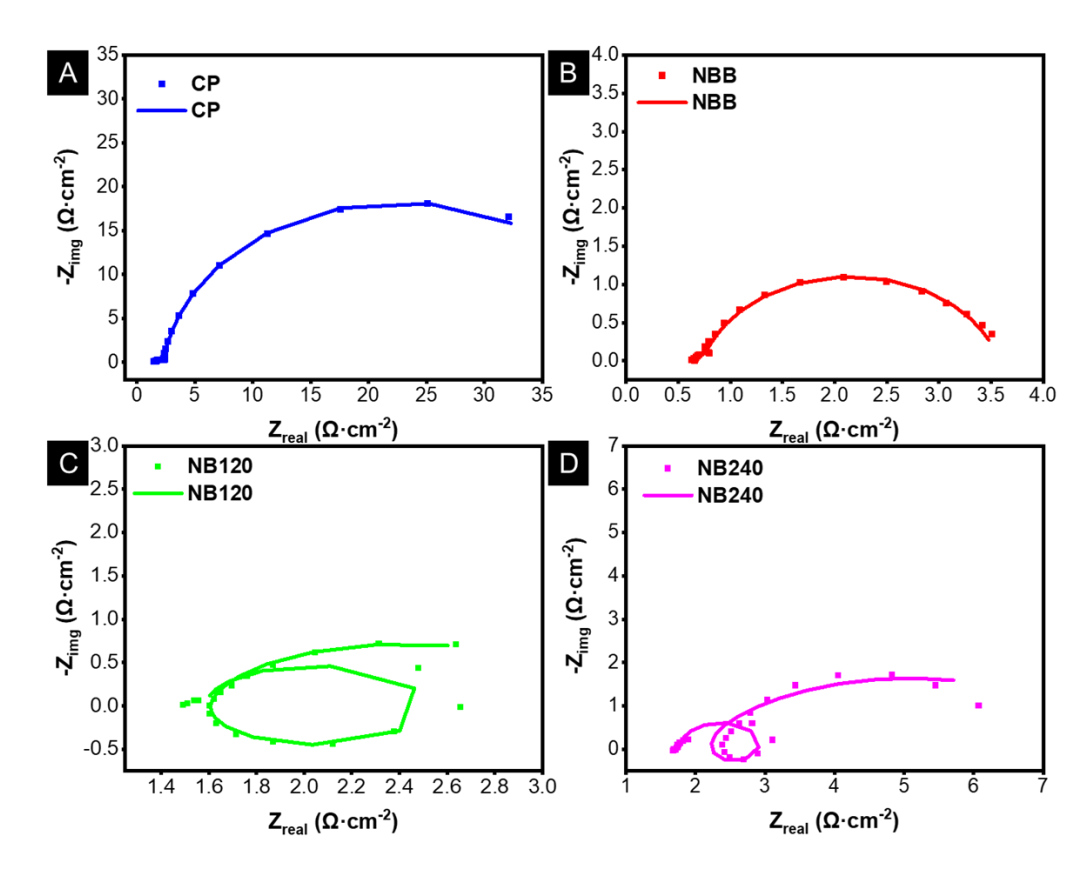


Figure 6. Nyquist plots of the EIS measurement for the produced Ni-B/CP electrodes.

structure transformed into a crystalline structure consisting of Ni matrix and Ni₃B precipitates. Generally, it was reported that the Ni-B amorphous structure possesses a superior catalytic performance in comparison with its crystalline counterpart. The presence of B as a dissolved species influences the electronic structure; this positively impacts the catalytic performance [31].

Also, heat treatment can affect the surface morphology considerably, as shown in Figure 8. The obtained structure in this figure includes some crystals with a size of 50 nm, having a high surface area, which makes the structure highly reactive. Moreover, a maximum ECSA of 48.5 was obtained for the heat-treated sample. Based on the obtained data, the effect of amorphous solid solution structure on the catalytic activity of Ni-B is dominant over the nanostructures with a high surface area, in such a way that with the formation of crystals and precipitations of Ni₃B, the catalytic performance will be suppressed.

However, in the same studies, it has been reported that heat treatment could play a role in enhancing the catalytic performance of the Ni-B layer if it is carried out in the temperature ranges that maintain the crystal structure unchanged [31] The as-deposited amorphous NiB possesses a high density of disordered surface sites, contributing to enhanced initial catalytic activity. Upon heat treatment, partial crystallization occurs (confirmed by XRD), leading to more ordered structures with reduced defect density. This correlates with the observed decrease in catalytic activity after annealing, as seen in the increased overpotential and reduced current density. Thus, the structural transition is directly reflected in the catalytic data, confirming that amorphous NiB is more active for OER under our conditions due to its higher surface reactivity and defect-rich nature. Table 4 provides a comparative demonstration of the same studies on the catalytic

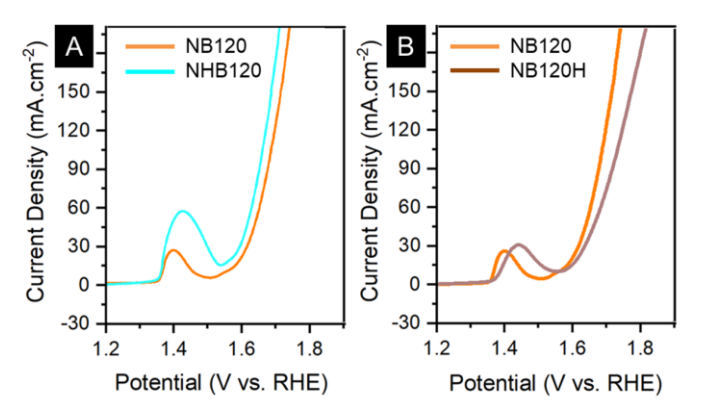


Figure 7. The LSV plots for the samples prepared with a deposition time of 120 s: a) effect of NaBH₄ concentration and b) effect of heat treatment at 500 °C.

behavior of binary Ni-B-based electrocatalysts. As illustrated in the table, the formation of uniform nanostructured Ni-B seeds on carbon papers can yield superior catalytic performance comparison to most Ni-B structures under other conditions [32-34]. The enhanced catalytic performance arises from the controlled synthesis method, which leads to uniform nanostructuring, optimized boron incorporation, and improved interaction with the carbon paper substrate. Compared to glassy carbon and nickel foam, carbon paper offers a unique combination of advantages. Unlike GC, which is flat and nonporous, carbon paper provides a porous and flexible structure that enhances catalyst loading and mass transport. In contrast to Ni foam, which may introduce background catalytic activity and interfere with measurements, carbon paper is chemically inert and electrically conductive, allowing for a more accurate evaluation of catalyst performance. Additionally, its high surface area and compatibility with nanostructured materials make it an ideal support for efficient electrocatalysis. All contributing to increased active surface area and better charge transfer kinetics compared to previously reported Ni-B materials.

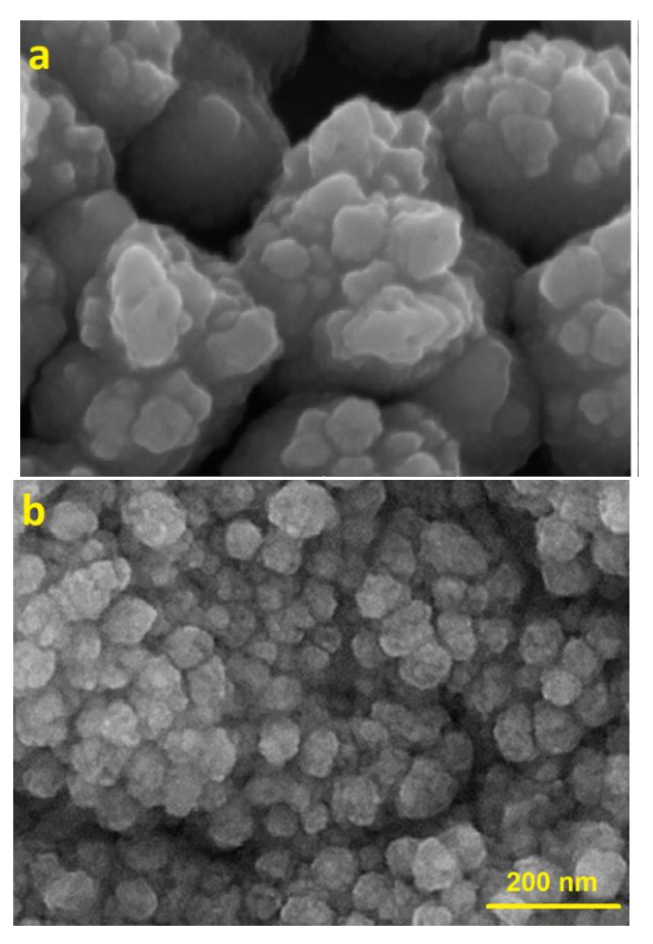


Figure 8. The effect of post-heat treatment on the surface morphology of the NB120 sample: a) before and b) after post-heat treatment.

4. Conclusions

The nanostructured Ni-B seed layer deposited on carbon paper was successfully evaluated for use as an electrocatalyst for OER by the low-cost electroless deposition method. Results show that the OER overpotential decreased with the increment of deposition time. The rise of deposition time to 240 s resulted in the formation of new nuclei on the previously formed layer, which led to a decrease in active surface and thus catalytic performance. And by raising of B concentration dissolved into the Ni-based deposited layer matrix, the catalytic properties promoting have enhanced. Despite crystallization and augmenting the surface area, heat treatment at 400 °C for 1 h resulted in the catalytic performance diminishment due to the formation of the Ni₃B phase. The best catalytic properties were obtained via the formation of a uniform layer of nanostructure seed layer after 120 s of electroless deposition time. To enhance the practical relevance of these findings, future research should also address the long-term stability and durability of the catalysts under operational conditions.

Acknowledgments

The authors acknowledge financial support from Iran National Science Foundation (INSF, Grant number 99022418).

CRedit Author Statement

Author Contributions: Taghi Morshedlo: Invegation, Data curation, Visualization, Writing - Original Draft, Writing - Review & Editing. Seyed Alireza Hosseini: Conceptualization, Supervision, Validation, Resources, Visualization, Writing - Original Draft, Writing - Review & Editing, Project administration, Funding acquisition. Soghra Ghorbanzadeh: Investigation,

Data curation, Visualization, Writing - Original Draft, Writing - Review & Editing. Mohammad Hossein Shahini: Investigation, Data curation, Visualization, Writing - Original Draft, Writing - Review & Editing. Mostafa Alishah: Investigation, Data curation, Visualization, Writing - Original Draft, Writing - Review & Editing. All authors have read and agreed to the published version of the manuscript.

References

- [1] Madhumitha, A., Preethi, V., Kanmani, S. (2018). Photocatalytic hydrogen production using TiO₂ coated iron-oxide core shell particles. *International Journal of Hydrogen Energy*, 43(8), 3946-3956. DOI: 10.1016/j.ijhydene.2017.12.127
- [2] McCrory, C.C., Jung, S., Ferrer, I.M., Chatman, S.M., Peters, J.C., Jaramillo, T.F. (2015). Benchmarking hydrogen evolving reaction and oxygen evolving reaction electrocatalysts for solar water splitting devices. J. Am. Chem. Soc., 137(13), 4347-4357. DOI: 10.1021/ja510442p
- [3] Ghorbanzadeh, S., Hosseini, S.A., Alishahi, M. (2022). CuCo2O4/Ti3C2Tx MXene hybrid electrocatalysts for oxygen evolution reaction of water splitting. *Journal of Alloys and Compounds*, 920, 165811. DOI: 10.1016/j.jallcom.2022.165811
- [4] Ghorbanzadeh, S.H., Taghdiri, S.A., Alishahi, A. M. (2022). Water oxidation electrocatalyst: A new application area for Ruthner powder waste material. Boletin De La Sociedad Espanola De Ceramica Y Vidrio, 61(4), 336-346. DOI: 10.1016/j.bsecv.2021.01.002
- [5] Masa, J., Weide, P., Peeters, D., Sinev, I., Xia, W., Sun, Z., Somsen, C., Muhler, M., Schuhmann, W. (2016). Amorphous cobalt boride (Co₂B) as a highly efficient nonprecious catalyst for electrochemical water splitting: oxygen and hydrogen evolution. Advanced Energy Materials, 6(6), 1502313. DOI: 10.1002/aenm.201502313

Table 4. The comparison of the different studies' outcomes regarding the catalytic performance of the binary Ni-B structure on the different substrates.

Catalysts	Electrolyte	$\eta_{I0}(\mathrm{mV})$	Tafel Slope (mV.dec ⁻¹)	Reference
Ni-B nanorods on stainless steel	0.1 M KOH	382	45	[9]
Ni-B particles on graphene	1 M KOH	369 (@30 mA.cm ⁻²)	85.2	[32]
Ni-B nanoparticle film on Ni foam	1 M KOH	360 (@100 mA.cm ⁻²)	76	[13]
Ni-B nanoparticle film on GC electrode	1 M KOH	362	54	[33]
Ni-B nanoparticle on GC electrode	1 M KOH	338	48	[34]
Nanostructured Ni-B seeds on CP	1 M KOH	320	99	(This work)
Nanostructured Ni-B seeds on CP	1 M KOH	450 (@100 mA.cm ⁻²)	99	(This work)

- [6] Sun, M., Liu, H.J., Qu, J.H., Li, J.H. (2016). Earth-Rich Transition Metal Phosphide for Energy Conversion and Storage. Advanced Energy Materials, 6(13), 1600087. DOI: 10.1002/aenm.201600087
- [7] Riedel, W., Electroless Nickel Plating, ASM International, Metals Park Ohio. 1991, USA/Fnishing Publications Ltd., Stevenage, Hertfordshire, England.
- [8] Srinivasan, K.N., Meenakshi, R., Santhi, A., Thangavelu, P.R., John, S. (2010). Studies on development of electroless Ni-B bath for corrosion resistance and wear resistance applications. Surface Engineering, 26(3), 153-158. DOI: 10.1179/174329409x409468
- [9] Zeng, M., Wang, H., Zhao, C., Wei, J., Qi, K., Wang, W., Bai, X. (2016). Nanostructured Amorphous Nickel Boride for High-Efficiency Electrocatalytic Hydrogen Evolution over a Broad pH Range. ChemCatChem, 8(4), 708-712. DOI: 10.1002/cctc.201501221
- [10] Sheng, M., Wu, Q., Wang, Y., Liao, F., Zhou, Q., Hou, J., Weng, W. (2018). Network-like porous Co-Ni-B grown on carbon cloth as efficient and stable catalytic electrodes for hydrogen evolution. *Electrochemistry Communications*, 93, 104-108. DOI: 10.1016/j.elecom.2018.06.017
- [11] Huang, T., Shen, T., Gong, M., Deng, S., Lai, C., Liu, X., Zhao, T., Teng, L., Wang, D. (2019). Ultrafine Ni-B nanoparticles for efficient hydrogen evolution reaction. *Chinese Journal of Catalysis*, 40(12), 1867-1873. DOI: 10.1016/S1872-2067(19)63331-0
- [12] Zhang, P., Wang, M., Yang, Y., Yao, T., Han, H., Sun, L. (2016). Electroless plated Ni-B films as highly active electrocatalysts for hydrogen production from water over a wide pH range. Nano Energy, 19, 98-107. DOI: 10.1016/j.nanoen.2015.11.020
- [13] Edison, T.N.J.I., Atchudan, R., Karthik, N., Sethuraman, M.G., Lee, Y.R. (2017). Ultrasonic synthesis, characterization and energy applications of Ni-B alloy nanorods. *Journal of the Taiwan Institute of Chemical Engineers*, 80, 901-907. DOI: 10.1016/j.jtice.2017.07.034
- [14] Liang, Y.H., X.P. Sun, A.M. Asiri, Y.Q. He. (2016). Amorphous Ni-B alloy nanoparticle film on Ni foam: rapid alternately dipping deposition for efficient overall water splitting. *Nanotechnology*, 27(12), 12LT01. DOI: 10.1088/0957-4484/27/12/12lt01
- [15] Masa, J., Piontek, S., Wilde, P., Antoni, H., Eckhard, T., Chen, Y.T., Muhler, M., Apfel, U.F., Schuhmann, W. (2019). Ni-Metalloid (B, Si, P, As, and Te) Alloys as Water Oxidation Electrocatalysts. Advanced Energy Materials, 9(26), 1900796. DOI: 10.1002/aenm.201900796
- [16] Yilmaz, Y., Akbulut, H., Uysal, M. (2022). Effect of NaBH4 concentration on hardness and microstructural properties of electroless deposited St-37 steel. [Effect of NaBH4 concentration on hardness and microstructural properties of electroless deposited St-37 steel]. European Journal of Science and Technology, 39, 118-121. DOI: 10.31590/ejosat.1140395

- [17] Yunacti, M., Mégret, A., Staia, M.H., A Montagne, A., Vitry, V. (2021). Characterization of Electroless Nickel-Boron Deposit from Optimized Stabilizer-Free Bath. Coatings, 11(5), 576. DOI: 10.3390/coatings11050576
- [18] Delaunois, F., Lienard, P. (2002). Heat treatments for electroless nickel-boron plating on aluminium alloys. Surface & Coatings Technology, 160(2-3), 239-248. DOI: 10.1016/S0257-8972(02)00415-2
- [19] Rao, Q., Bi, G., Lu, Q., Wang, H., Fan, X. (2005). Microstructure evolution of electroless Ni-B film during its depositing process. *Applied Surface Science*, 240(1-4), 28-33. DOI: 10.1016/j.apsusc.2004.07.059
- [20] Okamoto, H., Massalski, T. (1990). Binary alloy phase diagrams. ASM International, Materials Park, Ohio, USA. December 1990. xxii, 3589 pp., 3 vol., the set. Adv. Mater., 3: 628-629. DOI: 10.1002/adma.19910031215
- [21] Tucker, R. (2013). ASM handbook, volume 5A: thermal spray technology. *Plastics Industry*, 335, 336. DOI: 10.31399/asm.hb.v05a.9781627081719
- [22] Chatti, M., Gardiner, J.L., Fournier, M., Johannessen, B., Williams, T., Gengenbach, T.R., Pai, N., Nguyen, C., MacFarlane, D.R., Hocking, R.K., Simonov, A.N. (2019). Intrinsically stable in situ generated electrocatalyst for long-term oxidation of acidic water at up to 80 C. Nature Catalysis, 2(5), 457-465. DOI: 10.1038/s41929-019-0277-8
- [23] Liang, Q.H., Brocks, G., Bieberle-Hutter, A. (2021). Oxygen evolution reaction (OER) mechanism under alkaline and acidic conditions. *Journal of Physics-Energy*, 3(2), 026001. DOI: 10.1088/2515-7655/abdc85
- [24] O'M, B. (1956). Kinetics of Activation Controlled Consecutive Electrochemical Reactions: Anodic Evolution of Oxygen. *Journal of Chemical Physics*, 24, 817-827. DOI: 10.1063/1.1742616
- [25] Suen, N.T., Hung, S.F., Quan, Q., Zhang, N., Xu, Y.J., Chen, H.M. (2017). Electrocatalysis for the oxygen evolution reaction: recent development and future perspectives. *Chem. Soc. Rev.*, 46(2), 337-365. DOI: 10.1039/c6cs00328a
- [26] Sun, K., Wang, K., Yu, T., Liu, X., Wang, G., Jiang, L., Bu, Y., Xie, G. (2019). Highperformance FeCoP alloy catalysts by electroless deposition for overall water splitting. *International Journal of Hydrogen Energy*, 44(3), 1328-1335. DOI: 10.1016/j.ijhydene.2018.11.182
- [27] Anantharaj, S., Chatterjee, S., Swaathini, K.C., Amarnath, T.S., Subhashini, E., Pattanayak, D.K., Kundu, S. (2018). Stainless Steel Scrubber: A Cost-Efficient Catalytic Electrode for Full Water Splitting in Alkaline Medium. ACS Sustainable Chemistry & Engineering, 6(2), 2498-2509. DOI: 10.1021/acssuschemeng.7b03964

- [28] Anantharaj, S., Venkatesh, M., Salunke, A.S., Simha, T.V.S.V., Prabu, V., Kundu, S. (2017). High-Performance Oxygen Evolution Anode from Stainless Steel via Controlled Surface Oxidation and Cr Removal. ACS Sustainable Chemistry & Engineering, 5(11), 10072-10083. DOI: 10.1021/acssuschemeng.7b02090
- [29] Sheng, M.Q., Weng, W., Wang, Y., Wu, Q., Hou, S. (2018). Co-W/CeO composite coatings for highly active electrocatalysis of hydrogen evolution reaction. *Journal of Alloys and Compounds*, 743, 682-690. DOI: 10.1016/j.jallcom.2018.01.356
- [30] Laszczyńska, A., Szczygieł, I. (2020). Electrocatalytic activity for the hydrogen evolution of the electrodeposited Co–Ni–Mo, Co–Ni and Co–Mo alloy coatings. *International Journal of Hydrogen Energy*, 45(1), 508-520. DOI: 10.1016/j.ijhydene.2019.10.181
- [31] Masa, J., Sinev, I., Mistry, H., Ventosa, E., Mata, M.D.L., Arbiol, J., Muhler, M., Roldan Cuenya, B., Schuhmann, W. (2017). Ultrathin High Surface Area Nickel Boride (NiB) Nanosheets as Highly Efficient Electrocatalyst for Oxygen Evolution. Advanced Energy Materials, 7(17), 1700381. DOI: 10.1002/aenm.201700381

- [32] Tang, W., Liu, X., Li, Y., Pu, Y., Lu, Y., Song, Z., Wang, Q., Yu, R., Shui, J. (2020). Boosting electrocatalytic water splitting via metalmetalloid combined modulation in quaternary Ni-Fe-PB amorphous compound. *Nano Research*, 13, 447-454. DOI: 10.1007/s12274-020-2627-x
- [33] Liu, G., He, D., Yao, R., Zhao, Y., Li, J. (2018). Amorphous NiFeB nanoparticles realizing highly active and stable oxygen evolving reaction for water splitting. *Nano Research*, 11(3), 1664-1675. DOI: 10.1007/s12274-017-1783-0
- [34] Lao, J., Li, D., Jiang, C., Luo, R., Peng, H., Qi, R., Lin, H., Huang, R., Gin, W., Luo, C. (2020). Efficient overall water splitting using nickel boride-based electrocatalysts. *International Journal of Hydrogen Energy*, 45(53), 28616-28625. DOI: 10.1016/j.ijhydene.2020.07.171